Characterization of Stabilization Conditions for PahZ2$_{KT-1}$

by

Marriah G. Gonzalez

A Thesis Submitted in Partial Fulfilment of the Requirements for the Degree of

Master of Science in Chemistry

Middle Tennessee State University

May 2022

Thesis Committee:

Dr. Justin M. Miller, Chair

Dr. Kevin Bicker

Dr. Paul Kline

ABSTRACT

Poly(aspartic acid) (PAA) is a biodegradable water-soluble synthetic polypeptide often used as a replacement for environmentally persistent polycarboxylates used in a wide-range of industrial and biomedical applications.[1,2,3] PAA was found to be degraded by two bacterial strains isolated from river water, *Sphingomonas* sp. KT-1 and *Pedobacter* sp. KP-2.[1,3] Two enzymes purified from *Sphingomonas* sp. KT-1 are responsible for the hydrolytic degradation of PAA into smaller aspartic acid units.[4] Poly(aspartic acid) hydrolase-1 ($PahZ1_{KT-1}$) is an endopeptidase that cleaves β-amide linkages, peptide bonds between β-amino acids, while Poly(aspartic acid) hydrolase-2 ($PahZ2_{KT-1}$) is an exopeptidase responsible for both α-amide, peptide bond between α-amino acids, and β-amide cleavage.[2] Understanding conditions that stabilize $PahZ2_{KT-1}$ may allow for protein engineering efforts that can enhance catalytic efficiency of tPAA degradation. It is reported here that with the introduction of NaCl, $PahZ2_{KT-1}$ was seen to sample a larger variety of conformational states through size-exclusion chromatography and dynamic light scattering (DLS) experiments. Limited proteolysis and protein unfolding experiments visualized by fluorescence spectroscopy demonstrated that protein stability was independent of NaCl concentration. However, reactions containing Zn(II) were found, through limited proteolysis and unfolding experiments, to display increased stability. DLS also demonstrated an increased $PahZ2_{KT-1}$ particle diameter from 9 ± 1 nm without the addition of zinc and 157 ± 13 nm with the addition of zinc. Lastly, binding affinities were determined by varying concentrations of zinc and produced a K_d within the nanomolar range.

TABLE OF CONTENTS

LIST OF FIGURES

CHAPTER I: INTRODUCTION

Polymers in Society

Polymers are found within every corner of society, from the plastic cup used to drink your Starbucks, to the epoxy used for the latest TikTok trend. Most plastics produced are used for packaging and are commonly derived from fossil hydrocarbons. These water-insoluble hydrocarbon polymers are generally stable which cause them to be non-biodegradable. [5,6] It is estimated that over 8000 million metric tons of plastic has been produced to date. Of the plastic produced each year, only 9% will be recycled, 12% will be incinerated, and 79% will accumulate in landfills and the natural environment.[5] With most plastics accumulating in landfills and the environment, the concern of increased environmental contamination arises and so does the search for biodegradable alternatives.[5]

Many synthesized products do not readily decompose allowing for the accumulation of plastics in landfills and natural environment. While the accumulation of macroplastics has demonstrated a need for biodegradable alternatives, what about polymers on the microscale and beyond? Microplastics are generally formed by the fragmentation of macroplastics by UV light. While water-soluble polymers (WSPs), well beyond the microscale, are directly and indirectly introduced into the environment.[5]

Water-soluble polycarboxylates, such as homopolymers of acrylic acid and copolymers of acrylic and maleic acid, are used in household cleaning products and detergents as dispersants and thickeners. [6,7] These polycarboxylate containing products disposed of “down-the-drain” enter the aqueous environment largely via industrial effluents, outflow of liquid waste or sewage into a river or the sea, and via expelled treated industrial process water.[6] Catanionic polyacrylamide copolymers (PAMs), water-soluble

polymer often used as flocculants in waste treatment, enter the environment primarily through recycled sludge used on agricultural land and treated wastewater run-off. [6,8] The previously mentioned WSPs demonstrate slow biodegradation causing concern for environmental accumulation[9-10] While WSPs are generally considered non-toxic, potential ecological effects may be associated with their function as flocculants, detergents, and water/soil conditioners in unintended environments.[2] However, the degradation of PAM by the release of neurotoxic acrylamide monomers is also a major cause for concern.[11]

Environmentally friendly alternatives are being increasingly studied for the replacement of persistent and potentially toxic polymers. One example being poly(aspartic acid), an eco-friendly biodegradable alternative to petroleum-derived non-biodegradable polycarboxylates. Poly(aspartic acid) has applications in agriculture, water treatment, pigment industry, and medicine.[2, 22]

Polycarboxylate Properties

Polycarboxylates have a wide range of applications in industrial, medical, and agricultural settings.[12, 13] They are commonly used in detergents as scale inhibitors or dispersants, in paper and cosmetics as thickening agents, in waste treatment as flocculants, and in medicine as the workhorse for drug delivery.[13,14] These wide range of uses are due to properties such as high solubility in water and high electrostatic interactions.[15,16] The polycarboxylate structure is composed of ionogenic functional groups along a polymeric chain that allow the polymer to become highly charged once placed in an ionizing solvent.[13,15,16] The functional groups bound to the carbon-carbon backbone not only determine the structure and function, but also attribute to the overall negative charge of anionic polycarboxylates.[7]

While it is advantageous that polycarboxylates are used for a wide range of applications, their biodegradability sets them at a disadvantage. Commonly used polycarboxylates have a molecular weight (Mw) that ranges from 2,000 to 70,000, dependent on functional groups used to compose the structure, and are composed of branched units. Polymers with higher a Mw and branched units degrade at slower rates than those with a lower Mw and smaller degree of branching.[7] In fact, commonly used polycarboxylates have been found to be environmentally stable and undergo little to no degradation. The lack of biodegradation of polycarboxylates, such as poly(acrylic acid) and its copolymers, is of interest since these were introduced in the 1980s as a replacement for polyphosphates in detergents. Phosphate buildup in rivers caused eutrophication as excess nutrients enhanced plant growth that led to death of animal life from the lack of oxygen. However, the accumulation of polycarboxylates causes acidic conditions to rise. While the acids used are non-toxic, long-term environmental effects must be considered. [6] Poly(amino aids), such as poly(aspartic acid), degrade into amino acid units that are neutral to the environment.

Poly(aspartic acid)

Poly(aspartic acid) (PAA) is biocompatible, biodegradable, and an eco-friendly anionic polycarboxylate.[19,20] PAA is synthesized by the thermal polymerization of L-aspartic acid into polysuccinimide units that are then ring opened upon hydrolysis using NaOH. The thermally synthesized product is referred to as tPAA and is composed of 70% β-amide units and 30% α-amide units.[19,21] Two bacterial strains isolated from river water, *Sphingomonas* sp. KT-1 and *Pedobacter* sp. KP-2, have been observed to degrade PAA.[1,3] Within *Sphingomonas* sp. KT-1, two enzymes were purified and found to be responsible

for the hydrolysis of PAA into a mixture of starting reactant and dimeric aspartic acid units.[4] The first enzyme characterized, Poly(aspartic acid) hydrolase-1 ($PahZ1_{KT-1}$), is responsible for β-amide cleavage while the second enzyme, Poly(aspartic acid) hydrolase-2 ($PahZ2_{KT-1}$), is responsible for both α- and β-amide cleavage.[2]

$PahZ1_{KT-1}$

Catalytically active $PahZ1_{KT-1}$ was found to assemble into a dimeric complex composed of two $PahZ1_{KT-1}$ monomers. Each monomer is assembled into an α/β hydrolase fold with a catalytic site composed of Ser157/Asp225/His280, a catalytic triad and assembly characteristic of serine proteases. The active sites were found oriented on opposites faces of the biologically active dimer, and an electrostatic map dimer highlighted a positively charged trough near the active site which is thought to aid in enzyme binding to anionic substrate, PAA.[2] Once substrate binds, $PahZ1_{KT-1}$ cleaves β-amide bonds via endo-type hydrolysis resulting in oligo(aspartic acid) units with a molecular weight of 200-1,000.[22] Complete degradation of poly(aspartic acid) into monomeric aspartic acid cannot be performed by $PahZ1_{KT-1}$ alone.[22]

$PahZ2_{KT-1}$

A second enzyme purified from *Sphingomonas* sp. KT-, $PahZ2_{KT-1}$, was found to degrade oligo(aspartic acid) into single aspartic acid units. [22] The catalytically active structure is similar to the $PahZ1_{KT-1}$ structure since both structures were found to assemble into homodimers.[1] Unlike $PahZ1_{KT-1}$, each $PahZ2_{KT-1}$ monomer is composed of two separate domains: a dimerization domain and a catalytic domain. The dimerization domain, like other protein/protein interfaces, contains nonpolar residues within the core of the dimer interface.[(1,53)] While the area near the active site contains a positively charged residues at

the surface, where negatively charged PAA may bind. Our lab recently found that PahZ2$_{KT-1}$ harbors two Zn^{2+} ions in the catalytic domain, characteristic of M28 metalloproteases. PahZ2$_{KT-1}$ functions as an exo-type hydrolase that cleaves both α- and β-amide bonds in oligo(aspartic acid) where aspartic acid units with a molecular weight around 133 are produced.[22]

M28 Metalloprotease

Reported structural comparisons using the DALI server revealed several structural homologues closely related to PahZ2$_{KT-1}$.[1] *Pseudomonas* sp. RS-16 carboxypeptidase G2 and *Haemophilus influenza* N-succinyl-l,l-diaminopimelic acid desuccinylase (DapE) are two experimentally characterized homologue structures that share 21% and 18% sequence identity with PahZ2$_{KT-1}$, respectively.[1,23] Both enzymes belong to a family known as M28 metallopeptidases which encompasses aminopeptidases (cleave peptide bonds from the N-terminus) and carboxypeptidases (cleave peptide bonds from the C-terminus).[23] Metalloproteases are frequently identified by the conserved active site motif HEXXH necessary for catalytic function and metal coordination.[24] Catalytic function of metalloenzymes occurs through the activation of water molecules for nucleophilic attack facilitated by one or two divalent ions, generally zinc.[t 24] Two zinc atoms are responsible for catalytic function in M28 metalloproteases.[23] Recent reports in our lab identified PahZ2$_{KT-1}$ as an M28 metalloprotease where co-catalytic zinc atoms bind to the Zn_I and Zn_{II} sites within the active site.[1] The primary sequence of PahZ2$_{KT-1}$ indicates the presences of two conserved motifs HXD and HXXD in the Zn_I and Zn_{II} sites, respectively.[1]

Like PahZ2$_{KT-1}$, carboxypeptidase G2 and DapE monomers were found to contain a dimerization domain and a catalytic domain.[1] Electrostatic surface potential maps demonstrated each of the enzymes, PahZ2$_{KT-1}$, carboxypeptidase G2 and DapE, were

composed of nonpolar residues at the core of the dimer interface.[1] While carboxypeptidase G2 and DapE contain negatively charged residues on the surface of the catalytic domain, unlike PahZ2$_{KT-1}$. Carboxypeptidase-G2 is a representative homolog for M28 proteases.[23] The active site is composed of conserved amino acid ligands bound to two co-catalytic zinc ions. The first zinc (Zn_I) is bound to ASP141, Glu176, and His386.[54] While the second zinc (Zn_{II}) amino acid is bound to Asp141, Glu200, and His112.[24,25,54] The crystal structure showed an activated water molecule and Asp141 bridge the two zinc ions.[23,24,54] A sequence alignment of Carboxypeptidase-G2 and PahZ2$_{KT-1}$ show conserved residues within the catalytic domain of both enzymes. The conserved amino acids aspartic acid, glutamic acid, and histidine in the Zn_I site and histidine and two aspartic acids in the Zn_{II} site.[1]

PahZ2$_{KT-1}$ Environmental Impact

Polymers impose a hazard on the environment as their continued use is found ubiquitously in everyday life. That is why it is important to not only study biodegradable compounds, but also how they are degraded. Microorganisms found in activated sludge have been used in municipal treatment plants to remove water-soluble biodegradable polymers, but complete removal is not always achieved as branched polymers with β-linkages decrease biodegradability.[8] Therefore, research must focus on enzymes found within microorganism that can degrade both α- and β- amide linkages.

Since PahZ2$_{Kt-1}$ catalyzes the cleavage of α- and β- amide linkages, understanding conditions that lead to an enhanced protein stability can lead to enhanced catalytic function where complete polymer degradation may occur. As mentioned previously, OAA is degraded into aspartic acid by PahZ2$_{Kt-1}$, but complete degradation does not always occur.

OAA was found to bind through electrostatic interactions and previous research performed has been in the absence of salts such as NaCl.[1] In biological environments, NaCl conditions are expected to be present, so understanding how catalytic activity is affected in such conditions is important for protein engineering. In addition, since PahZ2$_{Kt-1}$ has been reported as an M28 metalloprotease it is important to understand how varying zinc conditions may affect stability regarding enhanced protein function. The overall goal of this project was to study conditions that enhance PahZ2$_{KT-1}$ stability, which can lay a foundation for protein engineering for a more efficient means of polymer biodegradation.

CHAPTER II: EXPERIMENTAL

Materials

All solutions used to generate data reported here were prepared with double-distilled water produced from a Purelab Ultra Genetic System (Siemens Water Technology). The DNA coding for the mature PahZ2$_{KT-1}$ sequence was cloned into the pET15b vector using the 5' NdeI and 3' XhoI restriction sites. DNA synthesis and cloning was performed by GenScript (Piscataway, NJ).[1]

Protein Expression and Purification

The PahZ2$_{Kt-1}$ plasmid was transformed into BL21(DE3) *Escherichia coli* cells (New England Biolabs, Ipswich, MA). A single colony was used to inoculate 50 mL of

lysogeny broth (LB) media containing 50 μg/mL final carbenicillin. Cells were incubated overnight at 37 °C, shaking at 225 rpm. After incubation, 10 mL of this growth was used to inoculate 500 mL of LB-media in a 2 L Erlenmeyer flask where cells were grown to an optical density at 600 nm ($O.D._{600}$) equal to 1.0 at the same temperature and shaking. Expression of $PahZ2_{KT\text{-}1}$ was induced with 0.1 mM isopropyl β-D-1-thiogalactopyranoside (IPTG, GoldBio, St. Louis, MO) final and the flask was incubated at 20 °C for 4 hr with shaking at 250 rpm. The cells were harvested by centrifugation at 10,000 x g for 10 minutes at room temperature. Cell pellets were stored at -20 °C.

Pelleted cells were resuspended in 50 mM Tris (2-Amino-2-(hydroxymethyl)-1,3-propanediol) (p.H. = 8.0), 300 mM NaCl, 20 mM imidazole. Cells were lysed by sonication for 45 minutes on ice. Turbonuclease (50 uL, Accelagen, San Diego, CA) was added and allowed to rock for 45 minutes at room temperature to increase lysis and remove genomic DNA. The cell lysate was clarified by centrifugation at 10,000 x g for 20 minutes at 4°C and subsequently loaded to a HisPur Ni-NTA 5 mL cartridge (Thermo Scientific, Waltham, MA) equilibrated in 50 mM Tris (p.H. = 8.0), 300 mM NaCl, and 20 mM imidazole. After loading, $PahZ2_{KT\text{-}1}$ was eluted from the column with 50 mM Tris, 300 mM NaCl, and 500 mM imidazole using a gradient of 0 - 100% over 40 minutes. The eluted peak corresponding to $PahZ2_{KT\text{-}1}$ was collected and analyzed via SDS-PAGE which showed the protein was > 98 % pure after this single purification. Protein was dialyzed against 50 mM HEPES, pH 7.40 or 20 mM Tris, pH 8.0 and stored at 4 °C.[1]

Fluorescein-labeled β-tri(L-aspartic acid) Solid Phase Peptide Synthesis

Solid phase peptide synthesis was performed as reported elsewhere using Fmoc synthetic techniques.[55,56] The Fmoc/tBu approach is dependent on an orthogonal

protecting group mechanism. [55,56] Fmoc-L-aspartic acid-α-tert-butylester obtained from Chem Impex (Wood Dale, IL) was used to synthesize a β-linked aspartic acid tripeptide, β-D_3. The Fmoc group, a base-labile protecting group, was used to protect α-amino groups, and a t-butyl group, an acid-labile protecting group, was used to protect the α-carboxylic acid. The unprotected aspartic acid sidechain was left for peptide bond formation via a β-linkage. Deprotected Rink Amide polystyrene resin (0.8 mmol/g) was used as a solid support after swelling in 100% dimethylformamide (236 mg Rink Amide resin; 0.189 mmol). The aspartic acid monomers (L-aspartic acid-α-tert-butylester; 311.1 mg; 0.756 mmol) and resin were allowed to incubate for 10 minutes. N,N,N′,N′-tetramethyl-O-(1H-benzotriazol-1-yl)uronium hexafluorophosphate (HBTU; 286.7 mg; 0.756 mmol) in 5% N-methylmorpholine (NMM) in DMF was then added and rocked for 1 hour. Aspiration was used to remove excess liquid from the resin. DMF was used to wash the resin at least three times before ninhydrin testing was used calorimetrically to verify the success of the reaction. The resin was treated twice with 20% piperidine in DMF for 10 minutes to remove the Fmoc protecting group. Coupling reactions were evaluated using the ninhydrin-based Kaiser test and sequence verified by mass spectrometry.[57,58] Fluorescein isothiocyanate (FITC) was used to label the peptide in a 1.5-fold molar excess to yield Flu-β-D_3.

The resin was washed three times with CH_2Cl_2 and aspirated for 5-10 minutes to remove any excess DMF and FITC. Flu-β-D_3 was cleaved from the resin by incubation in 95% trifluoroacetic acid (TFA; 6.65 mL), 2.5% triisopropylsilane (TIS; 0.175 mL), and 2.5% H_2O (0.175 mL) for 1 hour. The cleavage solution was filtered to separate the resin from free Flu-β-D_3 and TFA was evaporated. A C18 spin column (Thermo Fisher, Waltham, MA) along with a step-gradient of water to 70 % acetonitrile containing 0.05%

trifluoroacetic acid was used to purify the fluorescent dyed peptide. The purified solution was lyophilized and stored at -20 °C until use.

Limited Proteolysis Tests Dynamic Behavior of PahZ2$_{KT-1}$ Conformation

Limited proteolysis experiments were performed as reported elsewhere and run in triplicate.[26] Briefly, all reactions were performed in buffer containing 50 mM K_2PO_4 (pH = 7.5 at 25 °C) and [NaCl] = 0.00, 0.25, or 0.50 M. PahZ2$_{KT-1}$ (2 μM) was incubated for 80 minutes with 25 nM Proteinase K using sample previously equilibrated in the presence of the designated [NaCl]. Samples were collected at 20-minute intervals and quenched with SDS sample-loading buffer (250 mM Tris HCl pH = 6.8, 8 % w/v sodium dodecyl sulfate, 0.1 % w/v bromophenol blue, 40 % v/v glycerol, and 200 mM 2-mercaptoethanol) supplemented with 10 mM phenylmethylsulfonyl fluoride before boiling at 100℃ for 10 minutes to ensure denaturation. Digestion products were separated using SDS-PAGE methods and visualized by coomassie staining.

Apparent Molecular Weight and Molecular Binding Behavior of PahZ2$_{KT-1}$ Determined by Size-exclusion Chromatography

Size-exclusion chromatography (SEC) experiments were performed to assess the dynamic behavior of PahZ2$_{KT-1}$ when introduced to conditions containing salt. Reaction samples contained 0.75 mg/mL PahZ2$_{KT-1}$ incubated in 50 mM HEPES pH 7.0 in the presence and absence of 500 mM NaCl overnight at 25 ºC. Samples were then injected on an GE AKTA Purification system equipped with a HiLoad 26/60 Superdex 200 pg column for analysis. Molecular weights were estimated using a previously constructed standard curve built with characterized globular proteins. To test molecular binding effects caused by the introduction of NaCl, 0.75 mg/mL PahZ2$_{KT-1}$ was incubated overnight at 25 ºC in

50 mM HEPES pH 7.0, +/- 500 mM NaCl, with or without fluorescein-labled β-tri(L-aspartic acid). Fluorescence data was used to observe binding behavior.

Dynamic Light Scattering Determines PahZ2$_{KT-1}$ Dimeric Integrity

To establish whether differing concentrations of NaCl would disturb the PahZ2$_{KT-1}$ dimeric structure, PahZ2$_{KT-1}$ dialysis experiments were setup with NaCl concentrations of 0 mM, 150 mM, and 500 mM in 50 mM HEPES, pH 7.0. Dialyzed solutions had a final concentration of 0.5 mg/mL and centrifuged at 17,000 x g for 5 minutes at room temperature to remove any particulate. A Zetasizer Nano ZS (Malvern Panalytical, Westborough, MA) with a size detection range of 0.3 nm to10 µm was used to analyze 500 µL aliquots of the protein solutions placed in disposable cells.[1] DLS experiments were also run to determine if the presence of Zn affected dimeric structure of PahZ2$_{KT-1}$. Reactions were prepared as previously mentioned without the presence of NaCl and in the presence and absence of 2 mM $ZnCl_2$.

PahZ2$_{Kt-1}$ [Gnd HCl] Dependent Unfolding Experiments

Unfolding experiments were performed to determine whether varying concentrations of NaCl would affect protein dynamics upon denaturation with Guanidine HCl (Research Products International, Mt. Prospect, IL). Samples were prepared by the incubation of 2 µM PahZ2$_{KT-1}$ in 50 mM K_2PO_4 (pH = 7.5 at 25 °C) for 3 hours with [NaCl] = 0.00, 0.25, or 0.50 M and [Gnd HCl] = 0.00, 0.50, 0.75, 1.00, 1.50, 1.75, 2.00, 2.50, 2.75, 3.00, 3.50, or 3.75 M. Once samples reached equilibrium, they were analyzed using a F-4500 Fluorescence Spectrophotometer with an excitation wavelength of 295 nm. Reactions were then performed in the presence 500 pM, 1 nM, 500 nM, 1µM, or 10 µM $ZnCl_2$ (pH=

2.9 at 25 ºC). Samples containing zinc were prepared in 50 mM HEPES (pH = 7.5 at 25 °C). Unfolding experiments were run in triplicate.

CHAPTER III: RESULTS AND DISCUSSIONS

PahZ2$_{KT-1}$ Undergoes NaCl Induced Conformational Changes

Proteins are known to display dynamic behavior and undergo conformational changes about their most stable conformation corresponding to a low energy native state.[27] It was recently reported that NaCl promoted a conformational shift from an open-complex to a closed-complex resulting in increased catalytic activity by PahZ2$_{KT-1}$.[1] To characterize the relationship between PahZ2$_{KT-1}$ conformational dynamics and NaCl concentration, limited proteolysis reactions were run by incubating 2 μM PahZ2$_{KT-1}$ with 25 nM Proteinase K for 80 minutes at 25 ºC, where [NaCl] = 0, 0.25, or 0.50 M. Limited proteolysis experiments are incubated with low concentrations of proteases where enzymatic digestion is controlled by the stereochemistry and flexibility of protein substrate that binds the protease active site.[28, 29, 30] Because this method relies on substrate dynamics, it is often used to investigate conformational dynamics of protein structures in solution.[30]

Native proteins are often resistant to degradation by non-specific proteases because their moderately rigid conformation restricts the adaptability for binding the protease active site. [29, 30] However, native proteins have been found to undergo enzymatic digestion at one or few peptide bonds, typically at flexible loops or "hinge" regions that link structural domains, and not at secondary structures due to a lack of structural complementarity between substrate and enzyme. These cleaved protein fragments, or "nicked" proteins, are generally large, stable, and closely associated to resemble the original protein complex or cleaved into single domains of multi-domain proteins. [29, 30] Nicked proteins can either degrade into smaller peptides or resist further degradation dependent on fragment stability.[30]

Since limited proteolysis relies on substrate behavior, proteases with broad substrate specificity are chosen for digestion.[29] Proteinase K, used in reactions depicted in Figure 1a, is a subtilisin-like serine endopeptidase with a characteristic catalytic triad of Asp^{39}-His^{69}-Ser^{224}.[31, 32] Proteolysis reactions are controlled via protease inactivation by the addition of a denaturing solvent, such as SDS PAGE (Sodium dodecyl sulfate-polyacrylamide gel electrophoresis) sample buffer, or inhibition by the addition of protease inhibitors.[30]

Proteolysis reactions were incubated with 50 mM K_2PO_4 (pH = 7.5 at 25 °C), [NaCl] = 0.00, 0.25, or 0.50 M, 2 μM $PahZ2_{KT-1}$, and 25 nM Proteinase K for 80 minutes. Using sample previously equilibrated in the presence of the designated [NaCl]. Samples were collected at 15 μL aliquots and quenched at 20-minute intervals with SDS sample-loading buffer (250 mM Tris HCl pH = 6.8, 8 % w/v sodium dodecyl sulfate, 0.1 % w/v bromophenol blue, 40 % v/v glycerol, and 200 mM 2-mercaptoethanol) supplemented with

10 mM phenylmethylsulfonyl fluoride, a serine protease inhibitor, then boiled for 10 minutes at 100 ºC. Samples were subjected to analysis SDS-PAGE and visualized by Coomassie staining.

SDS-PAGE is often used to determine subunit molecular weight and composition of purified proteins.[34] This is because SDS, an anionic surfactant composed of a polar sulfate head and hydrophobic 12-carbon alkyl chain coats protein fragments with a negative charge in a similar charge/mass ratio and stabilizes the denatured state.[35] Samples were boiled at 100 ºC to insure non-covalent bonds were broken disrupting the quaternary, tertiary, and secondary protein structure. Reducing reagent 2-mercaptoethanol (200 mM) was added to SDS sample buffer to cleave disulfide bonds necessary for protein folding aiding in uniform fragment geometry. Disrupted fragments contain similar charge/mass ratio and migrate through the gel matrix towards the anode at rates inversely proportional to the log of their molecular weight. Therefore, denatured products are separated by size where smaller molecules have a faster migration rate than larger molecules, facilitating the interpretation of results. [36]

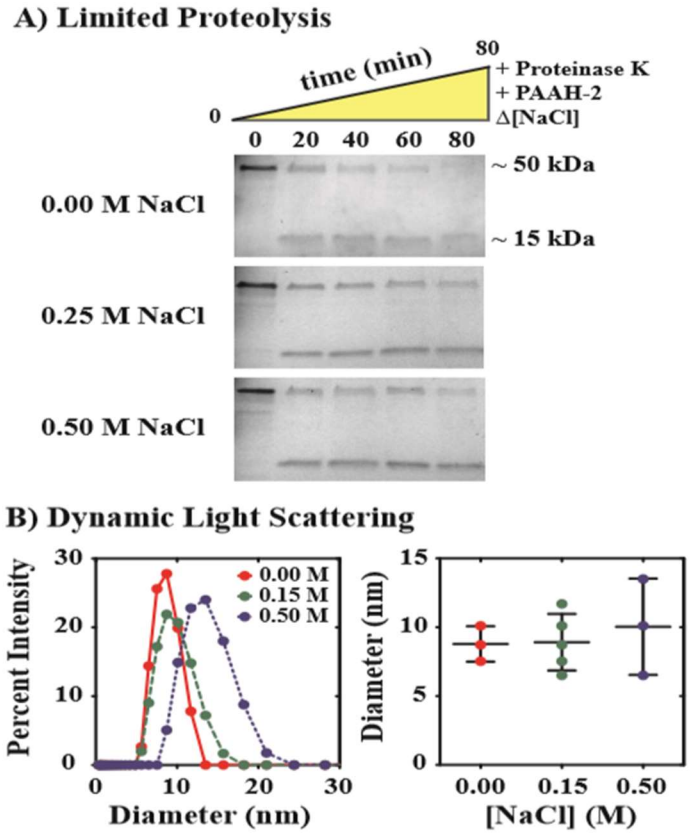

Figure 1. PahZ2$_{KT-1}$ undergoes a conformational change with the introduction of ionic solutions. (A) Limited proteolysis reactions were run in solutions containing [NaCl] = 0, 0.25, or 0.50 M and incubated with 2 µM PahZ2$_{KT-1}$ and 25 nM Proteinase K for 80 minutes at 25 ºC. Samples (15 µL) were quenched every 20 minutes and analyzed using SDS-PAGE. PahZ2$_{KT-1}$ monomers correspond to bands at 50 kDa while nicked protein fragments correspond to bands at 15 kDa. Intact PahZ2$_{KT-1}$ is seen to persist for 60 minutes in the absence of NaCl and at least 80 minutes in the presence of 0.25 and 0.5 M NaCl. With the introduction of NaCl, PahZ2$_{KT-1}$ displays a decreased sensitivity to proteinase K activity. (B) Dynamic light scattering experiments demonstrated that [NaCl] does not disturb dimer integrity. Samples analyzed by DLS were prepared with 0.5 mg/mL PahZ2$_{KT-1}$ in the addition of [NaCl] = 0, 0.15, and 0.5 M. The mean particle size observed for 0, 0.15, and 0.5 M NaCl were 8.78 ± 0.74, 8.91 ± 0.92, and 10.0 ± 2.0 nm, respectively.

Limited proteolysis reactions were performed in the presence of varying [NaCl] to determine its effect on the PahZ2$_{KT-1}$ dimer. In Figure 1a, SDS-PAGE analysis produced individual bands at 50 kDa and 15 kDa, which correspond to the PahZ2$_{KT-1}$ monomer and digested PahZ2$_{KT-1}$ fragments, respectively. At time zero, before digestion by proteinase K was allowed to take place, only one band is seen at 50 kDa in all reactions where [NaCl] =

0, 0.25, and 0.5 M. As mentioned previously, 50 kDa reflects the molecular weight of the PahZ2$_{KT-1}$ monomer, but, according to recent data the biological structure of PahZ2$_{KT-1}$ exists as a homodimer in solution. Therefore, SDS must be responsible for disruption at the dimer interface resulting in a band that corresponds to the molecular weight of a PahZ2$_{KT-1}$ monomer. A second band at 15 kDa is seen after 20 minutes of digestion with proteinase K and is thought to be the result of peptide bond hydrolysis at the hinge regions within the PahZ2$_{KT-1}$ structure. Complete digestion of PahZ2$_{KT-1}$ took place within 80 minutes in reactions without the addition of NaCl (Figure 1a). However, in the presence of 0.25 or 0.50 M NaCl monomers were seen to be intact at 60 and 80 minutes. The change in the rate of digestion is thought to be due to a conformational change induced by the introduction of NaCl in solution that produces a structure that is not as quickly degraded by proteinase K. NaCl was previously found to induce a conformational change from an open complex, in the absence of NaCl, to a closed PahZ2$_{KT-1}$ conformational state.[1]

Dynamic light scattering (DLS) experiments were performed to determine dimeric integrity of PahZ2$_{KT-1}$ when incubated with varied NaCl concentrations. DLS measures fluctuations in scattered light due to the random bombardment of particles in motion in a solution, or Brownian motion, which can be used to determine the hydrodynamic diameter, or overall average (z-average or cumulant average) particle diameter. [37] As particles move in solution, the constructive and deconstructive phases of scattered light will shift causing a shift in intensity. The Malvern Zetasizer Pro Blue measures the rate of change in intensity as a function of time and calculates particle size. Smaller particles will diffuse at faster rates; larger particles will diffuse at slower rates.[38]

DLS measurements were performed using 500 μL of 0.5 mg/mL PahZ2$_{KT-1}$ solutions where [NaCl] = 0, 0.15, and 0.5 M. Size distribution analysis found in Figure 1b as a plot of signal intensity as a function of particle diameter shows that in the absence of salt a mean particle diameter was equal to 8.8 ± 0.7 nm. Conditions where [NaCl] = 0.15 or 0.5 M the particle diameter was near 8.9 ± 0.9 and 10 ± 2 nm, respectively. Each condition was compared using the Student's *t* test and revealed no significant change among experiments. Peak width increased among conditions with 0 versus 0.5 M NaCl which indicates polydispersity, measure of the degree of heterogeneity of particle or molecular size and was quantitatively described by the increased standard deviation in the 0.50 M NaCl condition. However, pairwise *F*-tests suggest that all combinations of variance are statistically identical. Therefore, the combined data shown in Figure 1. indicate that all diameters are statistically the same.

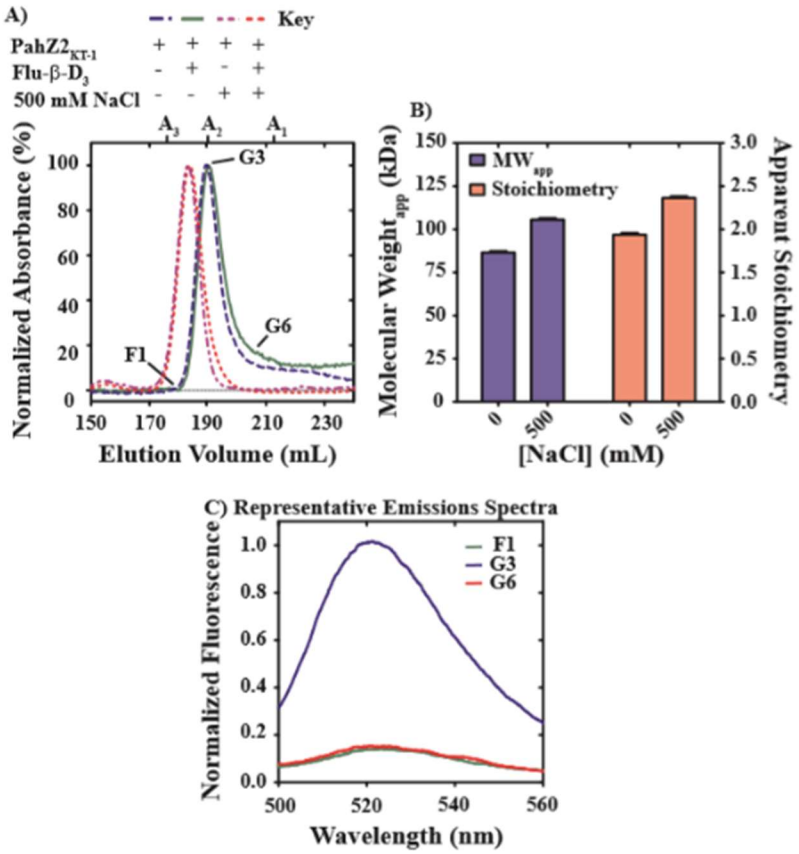

Figure 2. The shift in conformational dynamics of PahZ2$_{KT-1}$ induced by NaCl alters elution in size-exclusion chromatography. (A) Reactions were incubated with PahZ2$_{KT-1}$ in the presence or absence of NaCl overnight at 25 ºC. Dashed blue and solid green lines represent chromatograms produced by reactions incubated without the addition of NaCl in the absence and presence of Flu-β-D$_3$, respectively. Chromatograms represented by purple and red dashed lines were produced from reactions incubated with 500 mM NaCl in the absence and presence of Flu-β-D$_3$, respectively. Fractions labeled A_1, A_2, and A_3 represent elution volumes of predicted PahZ2$_{KT-1}$ monomers, dimers, and trimers, respectively. (B) Double-*Y* plot of apparent molecular weight and apparent stoichiometry obtained from reactions incubated in the presence and absence of 500 mM NaCl. (C) Emission spectra produced from fractions collected from SEC labeled F1, G3, and G6. Maximum fluorescence is produced by fraction G3 which represents the PahZ2$_{KT-1}$ dimeric species.

Prior to recent work done in our lab, all activity assays performed neglect the effect salt ions have on the hydrolysis of oligo(aspartic acid) by PahZ2$_{KT-1}$.[2] Proteolytic function of PahZ2$_{KT-1}$ occurs under physiological conditions that undoubtedly contain salt which was found to induce a conformational change from an open complex, when salt is absent,

to a closed complex, when NaCl is present.[2] The conformational change was expected to effect anionic substrate binding to the protein complex therefore, SEC experiments were run complimentary to DLS experiments to assess the dynamic behavior induced by NaCl. Samples analyzed by SEC were prepared by the overnight incubation of 0.75 mg/mL $PahZ2_{KT\text{-}1}$ with [NaCl] = 0 or 0.5 M at 25 C°. Elution through the SEC column was achieved under buffer conditions where [NaCl] = 0 or 0.5 M. The resulting chromatograms were used to estimate protein molecular weight using a previously constructed standard curve built with characterized globular proteins.

The chromatograms for each reaction condition can be found in Figure 2 panel A where the dashed blue line represents the 0 M NaCl condition, and the dashed purple line represents the 0.5 M NaCl condition. Conditions incubated in the absence of NaCl are seen to elute later than conditions incubated with NaCl. The retention time of a molecule is based on the fraction of intraparticle pore volume that is accessible to the molecule or molecules being separated. This is because SEC columns are packed with a resin composed of particles with uniform pore sizes that allow for the separation of molecules based on size, where small molecules interact with the pores of the stationary phase while larger molecules elute between porous beads. Therefore, larger molecules will elute first, and smaller molecules will elute later.[39] Based on standard curves, fractions corresponding to A_1, A_2, and A_3 represent $PahZ2_{KT\text{-}1}$ monomers, dimers, and trimers, respectively. The introduction of NaCl was seen to promote a shift in elution volume indicating an increase in molecular weight. However, DLS data show that $pahZ2_{KT\text{-}1}$ is dimeric under both conditions indicating that the shift in SEC data is likely due to a shift in conformation to an open complex.

In Figure 2B, the estimated molecular weight of PahZ2$_{KT-1}$ is 86.6 ± 0.8 kDa in 0 M NaCl conditions and 106.6 ± 0.9 kDa in 0.5 M NaCl conditions. In the presence of NaCl, a shift in PahZ2$_{KT-1}$ complex stoichiometry is observed from 1.94 ± 0.02 to 2.4 ± 0.02 in 0 or 0.5 M NaCl conditions, respectively. While there is a shift in molecular weight, the shift in stoichiometry is not significant enough to assume an overall change in dimer assembly. The shift in elution volume may represent a shift in conformational dynamics that subsequently impacts elution through the size-exclusion column, where the salt induced closed complex elutes the column sooner than the open complex.

The chromatograms for each reaction condition can be found in Figure 2A where the dashed blue and solid green lines represent the 0 M NaCl condition with and without peptide bound, respectively, and the dashed purple and red lines represent the 0.5 M NaCl condition in the absence and presence of bound peptide, respectively. Conditions incubated in the absence of NaCl are seen to elute later than conditions incubated with NaCl. As seen in Figure 2A, the introduction of NaCl promoted a shift in elution volume indicating an increase in molecular weight, change in shape, or change in conformation. These data support the observed behavior that when NaCl is present, PahZ2$_{KT-1}$ undergoes a conformational shift from an open complex to a closed complex.[2] SEC data demonstrate that PahZ2$_{KT-2}$ forms a dimeric complex that is independent of [NaCl] while also demonstrating condition-dependent changes in dimer conformation. Data also indicates that the dimer can bind substrate weather NaCl is present or absent.

Our lab has previously reported that the introduction of NaCl promotes a shift in conformational dynamics that subsequently enhanced catalytic activity. Therefore, the effect NaCl introduces to protein substrate binding was observed using SEC experiments

run in the presence or absence of fluorescent labeled β-tri(L-aspartic acid) or Flu-β-D_3. Peptides of L-aspartic acid were synthesized because oPAA, or oligo(aspartic acid) is the known substrate for $PahZ2_{KT-1}$.[22] Fractions labeled F1, G3, and G6 were collected and show that the fraction labeled G3 emits the highest signal, which corresponds to the $PahZ2_{KT-1}$ dimeric complex bound to fluorescein-labeled peptide. Data also indicates that the dimer can bind substrate whether NaCl is present or absent. SEC data demonstrate that $PahZ2_{KT-2}$ forms a dimeric complex that is independent of [NaCl] while also demonstrating condition-dependent changes in dimer conformation.

$PahZ2_{KT-1}$ Stability is Independent of NaCl Induced Conformational Changes

Based on data reported here alongside simulation data, the addition of salt was observed to alter $PahZ2_{KT-1}$ conformation from an open complex to a closed complex while maintaining a dimeric structure.[1] $PahZ2_{KT-1}$ catalytic function also displayed an increase in activity with the introduction of NaCl.[1] Gnd HCl unfolding experiments were run to determine if salt induced conformational changes stabilized the protein complex resulting in an increased stability. $PahZ2_{KT-1}$ (2 μM) was incubated for 3 hours in 0.05 M HEPES with increasing [Gnd HCl] under variant conditions of [NaCl] = 0, 0.25, and 0.50 M. Tryptophan emissions were collected to monitor protein folding and the resulting spectral data was used to establish $K_{1/2}$, binding affinity, values to compare the degree of stability between $PahZ2_{KT-1}$ structures incubated in each salt condition.

Fluorescence Spectroscopy

Fluorescence spectroscopy is often used in biophysical techniques to study protein stability due to high sensitivity and detection without the use of radioactive labels.[40] There are three intrinsic fluorophores within protein structures: phenylalanine (phe, F), tyrosine

(tyr, Y), and tryptophan (trp, W) PahZ2$_{KT-1}$ unfolding experiments were analyzed using an excitation wavelength equal to 295 nm to ensure that fluorescence was produced by photons emitted from tryptophan residues alone.[41, 42] In protein fluorescence, tryptophan emissions are frequently used to understand protein structure due to its large extinction coefficient, absorption and fluorescence at longer wavelengths, and most importantly, emissions spectra that are solvent dependent.[43] Residues buried in the protein structure are likely in a non-polar environment, while the polarity of the environment of residues found on the surface depends on the solvent being used; in these experiments, a polar environment. Thus, as protein unfolding occurs, a signal change is expected due to change in solvent environment.

The structure, position, and intensity of fluorescence emissions spectra are sensitive to molecular conformation and symmetry. [40] Unlike phenylalanine and tyrosine, tryptophan fluorescence is sensitive to its solvent environment. Tryptophan emissions can occur from two isoenergetic transitions, ^1L_a in polar solvents and ^1L_b in non-polar solvents.[40] Emissions from the ^1L_b transition are structured mirroring the absorbance spectrum. In contrast, in a polar solvent where hydrogen bonding is present, emissions spectra are unstructured and shifted to longer wavelengths. The ^1L_a state has an increased solvent sensitivity as its transition involves the polar nitrogen atom of the indole ring and contains a large dipole moment compared to the ground state. [40, 41]

Tryptophan fluorescence behavior can be used to observe protein interactions such as conformational transitions, subunit association, substrate binding, and/or denaturation.[40] These interactions cause a shift in fluorophore transition from ground state to excited

statewhich effects the fluorescence intensity, polarization, and transition energy.[42] Protein interactions may also cause a shift in the microenvironment occupied by tryptophan residues which also result in spectral differences. [43, 40] A red shift is expected to occur as tryptophan residues are increasingly exposed to polar solvents due to hydrogen bonding of the imino nitrogen. As mentioned previously, the imino nitrogen is directly involved in the $^{1}L_{a}$ transition so red shifted peaks should appear unstructured. A blue shift indicates tryptophan residues exposed to an increasingly non-polar environment causing shielding from hydrogen bonding.

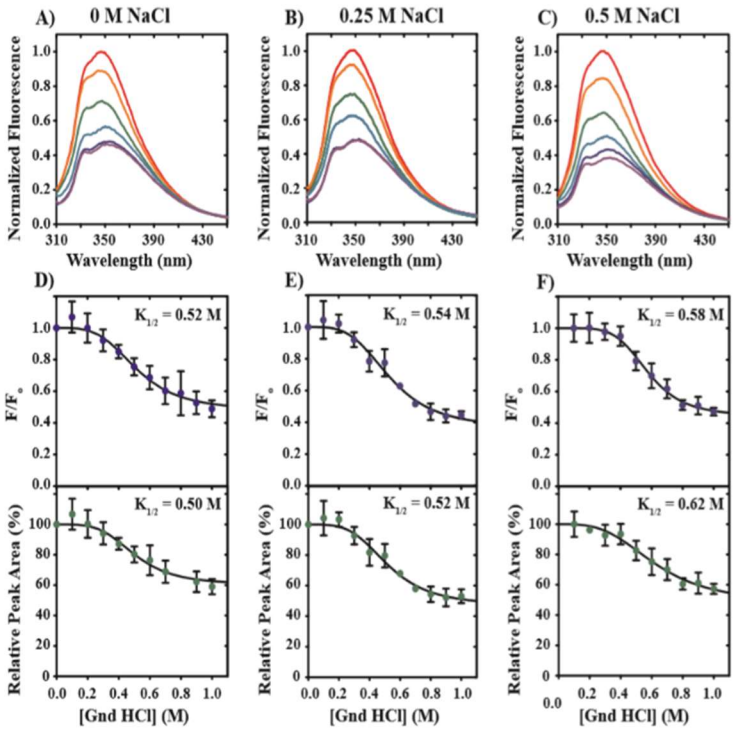

Figure 3. PahZ2$_{KT-1}$ stability is not dependent on [NaCl]. Unfolding experiments were prepared in 0.50 M HEPES and incubated with 2 uM PahZ2$_{KT-1}$ for 3 hours with [NaCl] and [Gnd HCl] as discussed previously. Normalized fluorescence data vs wavelength (nm) is shown for (A) 0 M NaCl (B) 0.25 M NaCl and (C) 0.5 M NaCl. Normalized fluorescence vs [Gnd HCl] (M) and relative peak area (%) vs [Gnd HCl] (M) are shown for each condition as well; (D) 0 M NaCl (E) 0.25 M NaCl and (F) 0.5 M NaCl. Data graphed in panels D-F were used to determine $K_{1/2}$ values.

[Gnd HCl] Protein Unfolding

Emission data observed in Figure 3 was produced by tryptophan residues found in PahZ2$_{KT-1}$, where each monomer contains a single tryptophan residue located in the catalytic domain near the active site. Tryptophan residues were expected to interact with their environment identically producing identical emission spectra. However, in each salt condition a peak and shoulder were observed which suggested two separate populations of tryptophan residues were present: one in a non-polar environment (ʎ = 330 nm) and the other in a completely polar environment (ʎ = 350 nm).[40] Differences in PahZ2$_{KT-1}$ conformational states from an open complex to a closed complex can explain differences

in the local environment surrounding tryptophan residues causing a shift in emissions data. Emissions spectra underwent a red shift in peak maxima as [Gnd HCl] increased indicating a change in electronic behavior of the two tryptophan populations. The change in emission behavior is thought to be caused by tryptophan residues becoming increasingly exposed to a polar solvent, and thus an increase in hydrogen bonding, as PahZ2$_{KT-1}$ unfolds.

In all spectra where a peak accompanied with a shoulder were observed, the peak seen at longer wavelengths has a greater intensity than the shoulder seen at shorter wavelengths. This can be explained by the mole fraction of tryptophan residues in two different environments causing a shift in excitation state. The lower intensity of the shoulder peak at shorter wavelengths could suggest there are fewer tryptophan residues in a non-polar environment compared to a greater population of tryptophan residues in a completely polar environment. This is because fluorescence intensity is directly related to fluorophore concentration. However, fluorescence intensity is also directly related to fluorophore quantum yield. Tryptophan residues located in non-polar solvents exhibit higher quantum yields than residues located in polar solvents. The change in quantum yield is due to hydrogen bonding of the imino nitrogen and stabilizing effects produced by the polar solvent on the increased dipole moment of the fluorophore in the excited state resulting in a shifted emission to lower energies. Therefore, the excitation of tryptophan should have produced higher emission intensities at shorter wavelengths rather than at longer wavelengths. The tryptophan residue located in the non-polar environment is likely partially or completely buried in the protein interior which could have been effected by nearby quenching from neighboring amino acids, such as lysine or histidine, upon relaxation from the excited state.[40] In all conditions, 0, 0.25, and 0.50 M NaCl, as [Gnd

HCl] increased, the peak intensities decrease. The peak intensity decreases as tryptophan is introduced to an increased polar solvent because the ^1L_a electronic transition moves to lower energies as polarity increases. Intensity of peak maxima is also affected by solvent quenching leading to the apparent decrease in PahZ2$_{KT-1}$ tryptophan emissions.

Guanidine hydrochloride unfolding curves are often used to approximate the stability of proteins by determining the differences in conformational stabilities between the native and unfolded states.[44] Increased $K_{1/2}$ values indicate that larger concentrations of denaturant are necessary for unfolding Therefore, conditions that promote midpoint increases are assumed to stabilize the protein against chemical denaturation. Stability was measured for each condition where $K_{1/2}$ values were determined to be 0.52, 0.54, and 0.58 M based on the normalized fluorescence for 0, 0.25, and 0.50 M NaCl, respectively. The relative peak area was also used to determine $K_{1/2}$ values for the three salt conditions with $K_{1/2}$ resulting in 0.50, 0.52, and 0.62 M for 0, 0.25, and 0.50 M NaCl, respectively. Data suggested there is no significant change in protein stability with the addition of NaCl.

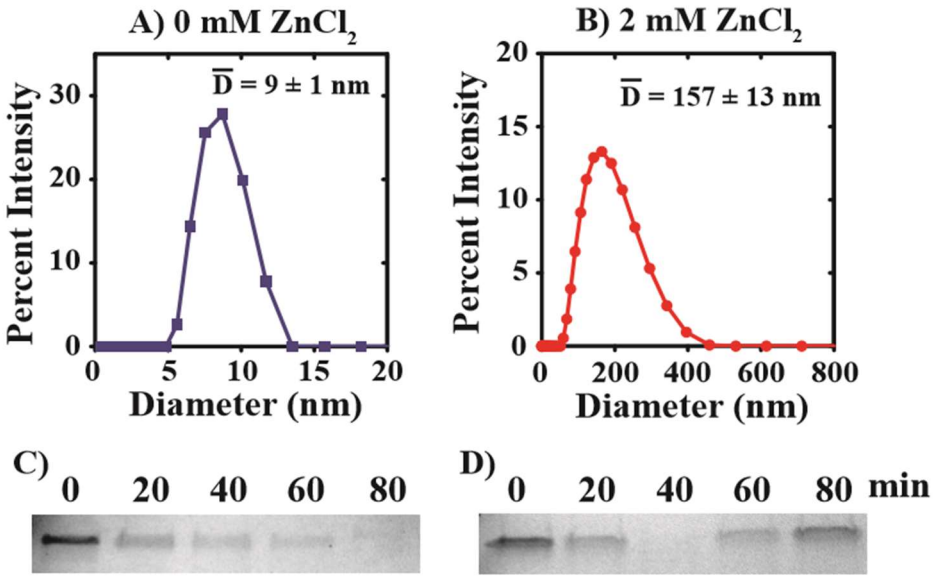

Figure 4. Zn(II) alters PahZ2$_{KT-1}$ diameter subsequently altering its stability against proteinase K digestion. Samples prepared for DLS contained 0.5 mg/mL PahZ2$_{KT-1}$ in the presence and absence of 2 mM $ZnCl_2$. (A) In the absence of Zn, PahZ2$_{KT-1}$ diameter was found to be 9 ± 1 nm. (B) In the addition of 2 mM $ZnCl_2$, the diameter of PahZ2$_{KT-1}$ was determined to be 157 ± 13 nm. (C) Limited proteolysis experiments displayed complete digestion of starting material within 80 minutes in the absence of Zn(II). (D) However, starting material was seen to be intact at 80 minutes in reactions containing 2 mM $ZnCl_2$

Zinc Dependent PahZ2$_{KT-1}$ Conformational Dynamics Influence Protein Stability

Reported structural comparisons using the DALI server revealed several structural homologues closely related to PahZ2$_{KT-1}$. *Pseudomonas* sp. RS-16 carboxypeptidase G2 and *Haemophilus influenza* N-succinyl-l,l-diaminopimelic acid desuccinylase (DapE) are two experimentally characterized homologue structures that share 21% and 18% sequence identity with PahZ2$_{KT-1}$, respectively. Both M28 metallopeptidases have been reported to assemble into a dimeric complex with two zinc atoms bound to the catalytic domain. Recent reports in our lab identified PahZ2$_{KT-1}$ as a M28 metalloprotease where co-catalytic zinc atoms bind to the Zn_I and Zn_{II} sites of the active site. Bound zinc atoms produce the greatest catalytic activity opposed to other metal ions or in the absence of supplemented

metal ions.[1] PahZ2$_{KT-1}$ was incubated with 0 or 2 mM $ZnCl_2$ to monitor structural differences between metal bound protein and protein without ligand bound using DLS. Data obtained from DLS experiments found in Figure 4 indicate a significant shift in mean particle diameter from 9 ± 1 nm when [$ZnCl_2$] = 0 mM to 157 ± 13 nm when [$ZnCl_2$] = 2 mM. A mean particle diameter near 10 nm indicated a dimeric species, as shown previously in Figure 2. The greatly larger mean particle diameter of 157 ± 13 nm of PahZ2$_{KT-1}$ incubated with $ZnCl_2$ indicated the formation of an aggregate species. Unlike the addition of NaCl, the presence of Zn(II) is seen to significantly impact protein diameter by a 17-fold increase.

PahZ2$_{KT-1}$ limited proteolysis experiments were performed to determine if the increase in protein complex diameter affected protein digestion by proteinase K. Sample preparation was followed as previously mentioned, except in this case [$ZnCl_2$] was altered. Digested products were visualized by SDS-PAGE and Coomassie staining. The SDS-PAGE gel in Figure 4C demonstrates that complete digestion of protein in the absence of supplemented zinc ions occurs before 80 minutes. Protein incubated with 2 mM $ZnCl_2$ demonstrated resistance to proteolysis even after 80 minutes. All proteolysis experiments were run in triplicate and representative gels are pictured. However, the formation of aggregate species made it difficult to produce SDS-PAGE gels that were uniform with respect to band position of digested products, suggesting the formation of an aggregate species that may not be ordered. Despite difficulties, SDS-PAGE gels run with reactions containing zinc were consistent in that intact PahZ2$_{KT-1}$ was seen at 80 minutes. Limited proteolysis reactions demonstrated that aggregate species of PahZ2$_{KT-1}$ dimer complexes

form in the addition of Zn^{2+} resulting in a complex that is not as readily digested by proteinase K.

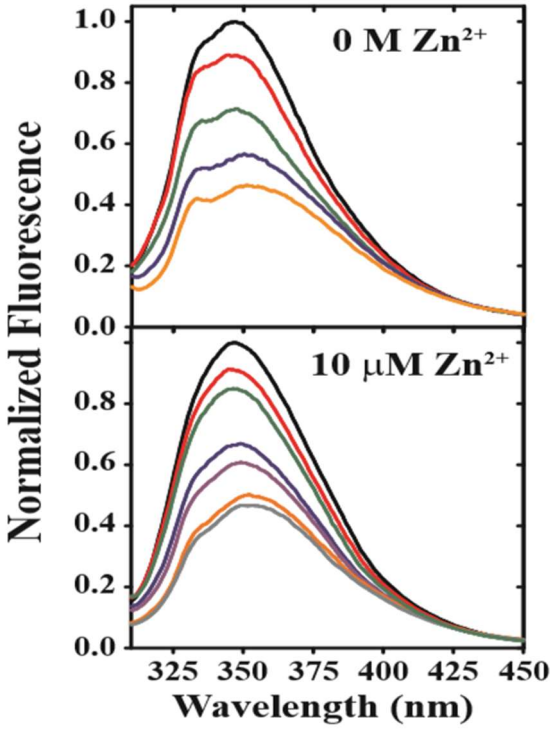

Figure 5. The incubation of $PahZ2_{KT-1}$ with Zn^{2+} alters tryptophan fluorescence signal. [Gnd HCl] dependent unfolding experiments were incubated with 2 μM $PahZ2_{Kt-1}$, [Zn^{2+}] = 0 or 10 μM. In the absence of Zn^{2+}, [Gnd HCl] = 0 – 1.0 M. However, with the addition of 10 μM Zn^{2+} the [Gnd HCl] = 0 – 3.75 M. Two peaks were observed for each reaction where [Zn^{2+}] = 0 M, but they were not present at lower [Gnd HCl] when [Zn^{2+}] = 10 μM.

Fluorescence spectroscopy was used to determine whether Zn^{2+} induced structural changes altered protein stability. Unfolding reactions were prepared by the incubation of 2μM $PahZ2_{KT-1}$ for 3 hours with [Gnd HCl] = 0-1.0 M in reactions without Zn^{2+} or [Gnd HCl] = 0-3.75 M in conditions containing 10 μM Zn^{2+}. A Hitachi F-4500 Fluorescence Spectrophotometer was used to monitor unfolding transitions from the native to unfolded

state using λ_{Ex}= 295 nm. The collected fluorescence intensity obtained from each condition, F, was normalized relative to the fluorescence intensity produced by the 0 M Gnd HCl condition, F_o, (F/F_o). A plot of normalized fluorescence as a function of wavelength is provided in Figure 5, where the top spectra were collected from conditions run in the absence of Zn^{2+} and the bottom spectra were collected from conditions run with 10 μM Zn^{2+}. Emission spectra represented by black lines in Figure 6 were collected from reactions that contained [Gnd HCl] = 0 M. These spectra produced the greatest signal intensity near 350 nm independent of [Zn^{2+}]. A shoulder was seen to appear near 330 nm with lesser intensity in all spectra where reactions were incubated with 0 M Zn^{2+}. The shoulder was absent for reactions supplemented with 10 μM Zn^{2+} and 0 – 2 M Gnd HCl, but when [Gnd HCl] was 3 M or greater, a shoulder with diminished intensity was observed at shorter wavelengths. Fluorescence spectra are dependent on whether the tryptophan residue is located in the protein interior, partially buried, or completely solvent exposed where peak maxima are expected near 300 nm, 335 nm, and 355 nm, respectively.[45] Therefore, the shoulder seen at 330 nm in Figure 5 represent tryptophan residues that are partially or completely buried while peaks seen at 350 nm represent tryptophan residues that are completely solvent accessible.

Tryptophan residues are typically found completely or partially buried in the interior of proteins due to its hydrophobic nature. [45] However, this is not always the case as demonstrated in Figure 5 where a population of tryptophan residues are completely solvent accessible. There are two tryptophan residues located in the PahZ2$_{KT-1}$ dimeric complex, one in each catalytic domain relatively close to the active site. the two tryptophan populations are likely explained by a catalytic domain that samples different

conformational states. When Zn^{2+} is added, one peak is seen in the absence and at low concentrations of denaturant. Therefore, the $PahZ2_{KT-1}$ structure is seen to undergo a conformational change where tryptophan residues are oriented towards the solvent.

In all cases, as [Gnd HCl] concentration increased, peaks demonstrated a red shift appearing at longer wavelengths with diminished intensity. A red shift indicates residues becoming increasingly exposed to polar solvent. A second trend is observed when [Gnd HCl] was at or greater than 3 M Gnd HCl or higher and 10 μM Zn^{2+} was added. A blue shifted peak was seen to appear near 330 nm where intensity decreased as denaturant increased. This second peak seen at shorter wavelengths represents tryptophan residues becoming increasingly exposed to a non-polar environment which can be explained by protein fragment crowding, nicked proteins form aggregates whose molecular properties are altered. [42,46]

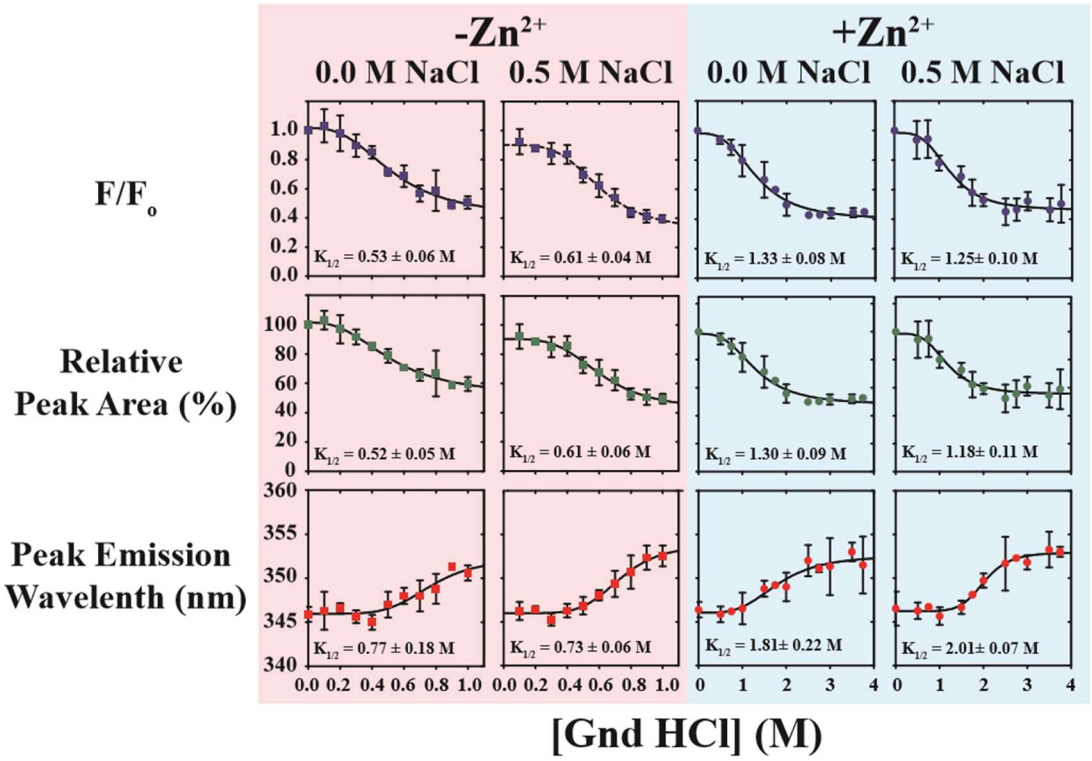

Figure 6. PahZ2$_{Kt-1}$ incubated with Zn^{2+} increases protein stability. Reactions were incubated with PahZ2$_{KT-1}$ in the presence and absence of NaCl and Zn^{2+}. Fluorescence data collected was plotted as a function of [Gnd HCl] and $K_{1/2}$ values were compared.

Stability values for protein unfolding experiments were quantitated because the observed increase in [Gnd HCl] necessary for protein unfolding to occur in the presence of 10 µM Zn^{2+} indicated an increase in protein stability (Figure 5). Therefore, $K_{1/2}$ values were determined by plotting F/F_o, relative peak area (%), and peak emission wavelength (nm) as a function of [Gnd HCl] for conditions where 2 µM PahZ2$_{KT-1}$ was incubated with 0 or 0.5 M NaCl and 0 or 10 µM Zn^{2+} (Figure 6). $K_{1/2}$ values were determined because ΔG values could not be directly determined for the irreversible unfolding of PahZ2$_{KT-1}$ by Gnd HCl.

Tryptophan in non-polar environment has a higher quantum yield, and as polarity increases, and thus hydrogen boding to the indole of tryptophan residues, the quantum yield decreases resulting in a diminished signal intensity. This trend was demonstrated by all reactions found in Figure 6. As the [Gnd HCl] increased, the peak intensity decreased which also resulted in a decrease in the relative peak area of the emission spectra. Also characteristic of tryptophan fluorescence, as the residues become solvent exposed and hydrogen bonding to the indole group increases, peaks shift to longer wavelengths as the ^1L_a transition is lower in energy. This trend is also demonstrated in Figure 6 for each reaction condition.

The emission trends seen for each reaction are noticeably similar in Figure 6. However, there is a significant difference in the $K_{1/2}$ values, [Gnd HCl] necessary for half unfolding to occur, when conditions in the absence of Zn^{2+} are compared to conditions containing Zn^{2+}. In the absence of Zn^{2+} the $K_{1/2}$ values range from 0.53 - 0.73 M with no significant difference when NaCl is present or absent. When Zn^{2+} is present, the $K_{1/2}$ values range from 1.33 – 2.01 M again with no significant difference when NaCl is present or absent. The $K_{1/2}$ values more than double in the presence of Zn^{2+} which suggests an increased stability . As previously stated, $PahZ2_{KT-1}$ is structurally similar to carboxypeptidase G2 and DapE, enzymes that are known to be dimeric with Zn^{2+} bound.[1] $K_{1/2}$ values support the claim that $PahZ2_{KT-1}$ is also a zinc metalloprotease.

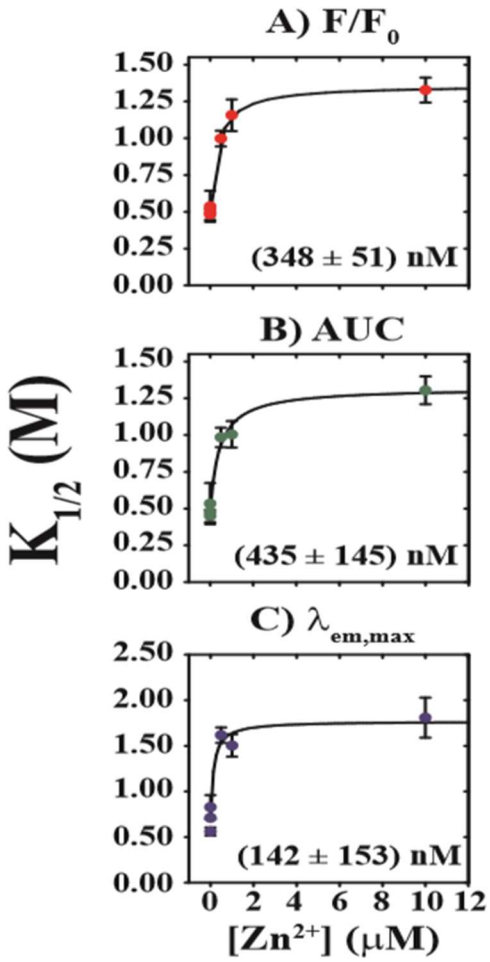

Figure 7. $K_{1/2}$ values determined from unfolding experiments were plotted against $[Zn^{2+}]$ to determine $PahZ2_{KT-1}$ binding affinity with zinc ions. (A) Normalized fluorescence data produced a K_d = 348 ± 51 nM. (B) Area under the curved data produced a K_d = 435 ± 145 nM. (C) Peak wavelength emission data produced a K_d = 142 ± 153 nM.

The specific recognition between protein and its ligands is essential in understanding enzymatic structure and function.[49] Fluorescence data collected from unfolding experiments incubated with several concentrations of Zn^{2+} were used to determine the Zn(II) binding affinity of $PahZ2_{KT-1}$. Binding affinity is defined as the strength of interaction between two or more molecules that bind reversibly, in this case ligand bound to protein. It is often expressed in terms of the dissociation constant (K_d),

which is the concentration of ligand that occupies half of the protein binding sites when equilibrium is reached. K_d values are used as a quantitative description of the strength of interaction between ligand (Zn(II)) and protein ($PahZ2_{KT-1}$).

The concentration of $PahZ2_{KT-1}$ was held at a constant concentration of 2 μM so that, when incubated with varying concentrations of Zn^{2+}, binding at equilibrium is independent of protein concentration. Protein and ligand were assumed to exist in the free or bound state only.[50]

K_d values for Zn^{2+} binding $PahZ2_{KT-1}$ were established using the binding curve found in Figure 7, where $K_{1/2}$ values determined from unfolding experiments were plotted against the concentration of Zn^{2+} used in the reactions. The plot demonstrates protein stability as Zn^{2+} binds $PahZ2_{KT-1}$, as the concentration of Zn^{2+} increased the protein became saturated and the concentration of the protein-ligand complex reached a plateau which indicated that upon saturation, stability of the protein was no longer affected by increased Zn(II) concentrations.[51] The K_d of protein binding metal ligand could be determined from the binding curve since it is defined as the concentration of ligand that leads to 50% occupancy of the protein binding site, as mentioned previously. Therefore, when the value on the Y-axis equaled $K_{1/2} \bullet 0.5$, K_d was equal to the corresponding X-axis value which was found to be 348 ± 51 nM (F/F_0), 435 ± 145 nM (AUC), and 142 ± 153 nM ($\lambda_{em, max}$). K_d values were seen to vary significantly between reactions run under the same conditions when differing Y parameters were used: normalized fluorescence intensity, area under the curve, or peak emission wavelength. However, all reported K_d values were within the nM range which leads to the assumption that the determined K_d is the result of binding at the Zn_{II} site, and not the Zn_I site since it's K_d was determined to be in the 16 pM.[1] This is

because the Zn_I site is assumed to be saturated at Zn^{2+} concentrations greater than the picomolar range and therefore would not demonstrate altered protein stability. Altered stability could have also been the result of Zn(II) binding at other sites along the protein other than the Zn_{II} site since the dissociation equilibrium was reported to be 49 nM.[1] Reactions run under differing Zn^{2+} concentrations are needed to fill gaps in data. The final shape of the graph, once gaps in data are filled, could help to determine binding cooperativity where a sigmodal graph indicates positive cooperativity, ligand binds protein increasing the affinity for another ligand to bind.[51]

CHAPTER IV: CONCLUSIONS

PahZ2$_{KT-1}$ was found to retain a dimeric complex composed of two identical subunits that contained a dimerization and catalytic domain. Recent work done by other members in the lab indicated that electrostatic interactions among the dimerization and catalytic domain were responsible for poly(aspartic acid) substrate binding to protein.[1] Data stated here indicated that an increase in NaCl concentration, and therefore increased electrostatic interactions, altered protein dynamics which was found to promote a shift in conformational dynamics where NaCl promotes a shift in the equilibrium between the open and closed states of PahZ2$_{KT-1}$.[1] This shift in PahZ2$_{KT-1}$ conformation was found to have little to no effect on protein stability demonstrating that stability was independent of NaCl concentration.

The PahZ2$_{KT-1}$ catalytic domain was reported to be an M28 metalloprotease where Zn^{2+} binds as a cofactor at the Zn_I and Zn_{II} site. The increase in Zn^{2+} concentration was found to alter protein conformation as demonstrated by DLS and fluorescence spectroscopy experiments. Limited proteolysis experiments run with proteinase K and unfolding reactions incubated with Zn^{2+} analyzed by fluorescence spectroscopy revealed that the change in protein conformation resulted in an increased stability against protein degradation. Lastly, the binding affinity of PahZ2$_{KT-1}$ with Zn^{2+} was found to be 348 ± 51 nM (normalized fluorescence data), 435 ± 145 nM (area under the curved data), and 142 ± 153 nM (peak wavelength emission data). This data along with data collected from DLS and unfolding experiments indicates that Zn^{2+} is binding PahZ2$_{KT-1}$ in areas other than the catalytic site resulting in oligomeric structures that result in increased stability. All data

obtained is helpful in the engineering of proteins responsible for the biodegradation of polycarboxylates.

Future work would be to determine oligomeric structures produced when Zn^{2+} concentration is increased. It could also be helpful to determine where Zn^{2+} is binding along the protein. Experiments run with differing metals could also help determine if Zn^{2+} provides a structure with the greatest stability. Lastly, lower Zn^{2+} concentrations could be added to fill the gaps in the binding curve graph to accurately determine binding affinity and shape of the graph. Data reported here can helps fill in the gaps of our understanding on how $PahZ2_{KT-1}$ behaves in diverse solvent/salt conditions and how $PahZ2_{KT-1}$ behaves in response to Zn(II) concentration. It is important to understand factors that influence $PahZ2_{Kt-1}$ stability, whether function is sustained or impaired, so the information can be used to influence protein engineering into an enzyme that is more effective and efficient in the biodegradation of microplastics such as poly(aspartic acid).

REFERENCES

1. Brambley, C.; Yared, T.; Gonzalez, M.; Jansch, A.; Wallen, J.; Weiland, M.; Miller, J. *Sphingomonas* sp. KT-1 PahZ2 Structure Reveals a Role for Conformational Dynamics in Peptide Bond Hydrolysis. *J. Phys. Chem. B.* **2021**, 125, 22, pp 5722-5739.
2. Brambley, C; Bolay, A.; Salvo, H.; Jansch, A.; Yared, T.; Miller, J.; Wallen, J.; Weiland, M. Structural Characterization of *Sphingomonas* sp. Kt-1 Pahz1-Catalyzed Biodegradation of Thermally Synthesized Poly(aspartic acid). *ACS Sustainable Chem. Eng.* **2020**, 8, 29, pp 10702-10713.
3. Tabata, K.; Kasuya, K.; Abe, H; Masuda, K.; Doi, Y. Poly(aspartic acid) degradation by *Sphingomonas* sp. Isolated from Freshwater. *Appl. Environ. Microbiol.* **1999**, 65, 9, pp 4268-4270.
4. Hiraishi, T.; Kajiyama, M.; Yamato, I.; Doi, Y. Genetic Analysis and Characterization of Poly(aspartic acid) hydrolase-1 from *Sphingomonas* sp. Kt-1. *Macromol Biosci.* **2004**, 4, 3, pp 330-339.
5. Geyer, R.; Jambeck, J.; Law, K. Production, Use, and Fate of All Plastics Ever Made. *Sci*. *Adv*. **2017**, 3.
6. Jop, K.; Guiney, P.; Christensen, K.; Silberhorn, E. Environmental Fate Assessment of Two Synthetic Polycarboxylate Polymers. *Ecotoxicol. Environ. Saf.* **1997**, 37, pp 229-237.
7. Polycarboxylates. *The Soap and Detergent Association.* **1996**.
8. Hennecke, D.; Bauer, A.; Herrchen, M.; Wischerhoff, E.; Gores, F. Cationic polyacrylamide copolymers (PAMs): environmental half life determination in sludge-treated soil. *Environ. Sci. Eur.* **2018**, 30, 16.
9. Buczek, S. B.; Cope, W. G.; McLaughlin, R. A.; Kwak, T. J. Acute toxicity of polyacrylamide flocculants to early life stages of freshwater mussels. *Environ. Toxicol. Chem.* **2017**, 36 (10), pp 2715− 2721
10. Thombre, S. M.; Sarwade, B. D. Synthesis and biodegradability of polyaspartic acid: A critical review. *J. Macromol. Sci., Part A: Pure Appl.Chem.* **2005**, 42, 1299.
11. Arp, H. P. H.; Knutsen, H. Could We Spare a Moment of the Spotlight for Persistent, Water-Soluble Polymers? *Environ. Sci. Technol*. **2019**, 54 (1), pp 3−5.
12. Nakato, T.; Yoshitake, M.; Mastubara, K.; Tomida, M. Relationships between Structure and Properties of Poly(aspartic acid)s. *Macromolecules*. **1998**, *31*, pp 2107-2113.
13. Opgenorth, HJ. Polymeric Materials Polycarboxylates. *Anthropogenic Compounds*, vol 3/3F. Springer, Berlin, Heidelberg, **1992**, pp 337-350.
14. Zhang, H.; Lin, Xinrong, L.; Chin, S.; Grinstaff, M. Synthesis and characterization of Poly(glyceric Acid Carbonate): A Degradable Analogue of Poly(acrylic Acid). *J. Am. Chem. Soc.* **2015**, *137*, pp 12660-12666.
15. Gao, C.; Haiyan, S. Facile Synthesis of Multiamino vinyl Poly(amino acid)s for Promising Bioapplications. *Biomacromolecules* **2010**, *11*, pp 3609-3616.

16. Meka, S.; Manprit, S.; Pichika, M.' Nail, S.; Kolapalli, V.; Kersharwani, P. A comprehensive review on polyelectrolyte complexes. *Elsevier*. **2017**, *22*, pp 1697-1706.
17. Cheng, H.; Smith, P.; Gross, R. Green Polymer Chemistry: A Brief Review. *ACS Symposium Series*. **2013**, pp 1-12.
18. Stetefeld, J.; McKenna, S.; Patel, T. Dynamic light scattering: a practical guide and applications in biomedical sciences. *Biophys. Rev.* **2016**, *8*, pp 409-427.
19. Tabata, K.; Kajiyama, M.; Hiraishi, T.; Abe, H.; Yamato, I.; Doi, Yoshiharu. Purification and Characterization of Poly(aspartic acid) Hydrolase from *Spingomonas* sp. KT-1. *Biomacromolecules*. **2001**, *2*, pp 1155-1160.
20. Hiraishi, T. Poly(asparticacid)(PAA) hydrolases and PAA Biodegradation:current knowledge and impact on applications. *Appl. Microbial. Biotachnol.* ***2016***, *100*, pp 1623-1630.
21. Tabata, K.; Abe, A.; Doi, Y. Microbial Degradation of Poly(aspartic acid) by Two isolated Strains of *Pedobacter* sp. and *Sphingomonas* sp. *Biomacromolecules*. **2000**, *1*, pp 157-161.
22. Hiraishi, T.; Kajiyama, M.; Yamato, I.; Doi, Y. Enzymatic hydrolysis of α- and β-Oligo(L-aspartic acid)s by Poly(aspartic acid) Hydrolases-1 and 3 from *Sphingomonas* sp. KT-1. *Macromolecular Bioscience*. **2004**, *4*, pp 330-339.
23. Rawlings, N. D.; Barrett, A. J.; Bateman, A. MEROPS: the database of proteolytic enzymes, their substrates and inhibitors. Nucleic Acids Res**. 2012**, *40*, pp 343−350.
24. Xiong, B.; Loss, R. D.; Shields, D.; Pawlik, T.; Hochreiter, R.; Zydney, A. L.; Kumar, M. Polyacrylamide degradation and its implications in environmental systems. npj Clean Water. **2018**, *1*, 17.
25. Auld, D. Catalytic mechanisms for metallopeptidases. *Handbook of Proteolytic Enzymes*. **2013**, pp 370-396.
26. Brambley, C.; Marsee, J.; Halper, N.; Miller, J. Characterization of Mitochondrial YME1L Protease Oxidative Stress-Induced Conformational State. *JMB*. **2019**, *431*, pp 1250-1266.
27. Fontana, A.; Fassina, G.; Vita, C.; Dalzoppo, D.; Zamai, M.; Zambonin, M. Correlation between Sites of Limited Proteolysis and Segmental Mobility in Thermolysin. *Biochemistry*. **1986**, *25*, 8.
28. Petrotchenko, E.; Borchers, C. Modern Mass Spectroscopy-Based Structural Proteomics. *Advances in Protein Chemistry and Structural Biology*. **2014**, *95*, pp 1876-1623.
29. Fontana, A.; Polverino de Laureto, P.; Filippis, V.; Scaramella, E.; Zambonin, M. Probing the partly folded states of proteins by limited proteolysis. *Folding & Design*. **1997**, *2*, 2, pp R17-R26.
30. Fontana, A.; Polverino de Laureto, P.; Filippis, V.; Scaramella, E.; Zambonin, M. Limited Proteolysis in the Study of Protein Conformation. *Proteolytic Enzymes*. **1997**, pp 253-279.
31. Hoseini-Koupaei, M.; Shareghi, B.; Saboury, A.; Davar, F.; Sirotkin, V.; Hoseini-Koupaei, M. H.; Enteshari, Z. Catalytic activity, structure, and stability of

proteinase K in the presence of biosynthesized CuO nanoparticles. *International Journal of Biological Macromolecules*. **2019**, *122*, pp 732-744.

32. Silva, C.; Vazquez-Fernandez, E.; Onisko, B.; Requena, J. Proteinase K and the structure of PrP^{Sc}: The good, the bad and the ugly. *Virus Research*. **2015**, *207*, pp 120-126.
33. Ren, Y.; Luo, H.; Huang, H.; Hakulinen, N.; Wang, Y.; Wang, Y.; Su, X.; Bai, Y.; Zhang, J.; Yao, B.; Wang, G.; Tu, T. Improving the catalytic performance of Proteinase K from *Parngyodontium album* for use in feather degradation. *International Journal of Biological Macromolecules*. **2020**, *154*, pp 1586-1595.
34. Garfin, D. One-Dimensional Gel Electrophoresis. *Methods in Enzymology*. **1990**, *463*, pp 497-513.
35. Jafari, M.; Mehrnejad, F.; Rahimi, F.; Asghari, S. M. The Molecular Basis of the Sodium Dodecyl sulfate Effect on Human Ubiquitin Structure: A Molecular Dynamics Simulation Study. *Scientific Reports*. **2018**, *8*.
36. Frisch, R.; Krause, I.; Electrophoresis. *Encyclopedia of Food Science*. **1993**, pp 2055-2062.
37. Dynamic light scattering as a relative tool for assessing the molecular integrity and stability of monoclonal antibodies. *Biotechnology and Genetic Engineering Reviews*. **2007**, *24*, pp 117-128.
38. Zetasizer Nano User Manual. *Malvern Instruments Ltd.* **2013**.
39. A Review Size-Exclusion Chromatography for the Analysis of Protein Biotherapeutics and Their Aggregates. *Journal of Liquid Chromatography & Related Technologies*. **2012**, *35*, pp 2923-2950.
40. Laowicz, J. *Principle of Fluorescence Spectroscopy*. Springer, **2006**.
41. Callis, P. ^1L_a and ^1L_b Transitions of Tryptophan: Applications of Theory and Experimental Observations to Fluorescence of Proteins. *Methods in Enzymology*. **1997**, *278*.
42. Berlman, I. *Handbook of Fluorescence Spectra of Aromatic Molecules*. Academic Press, **1971**.
43. Sinderwicz, P.; Li, X.; Yates, E.; Turnbull, J.; Lian, L.; Yu, L. Intrinsic tryptophan fluorescence spectroscopy reliably determines galectin-ligand interactions. *Scientific Reports*. **2019**, *9*.
44. Monera, O.; Kay, C.; Hodges, R. Protein denaturation with guanidine hydrochloride or urea provides a different estimate of stability depending on the contributions of electrostatic interactions. *Protein Science*. **1994**, *3*, pp 1984-1991.
45. Royer, C. Probing Protein Folding and Conformational Transitions with Fluorescence. *Chem*. *Rev*. **2006**, *106*, pp 1769-1784.
46. Steer, B.; Merrill, R. Characterization of an Unfolding Intermediate and Kinetic Analysis of Guanidine Hydrochloride-Induced Denaturation of the Colicin E1 Channel Peptide. *Biochemistry*. **1997**, 36, pp 3037-3046.
47. Rumfeldt, J.; Galvagnion, C.; Vassall, K.; Meiering, E. Conformational stability and folding mechanisms of dimeric proteins. *Progress in Biophysics and Molecular Biology*. **2008**, *98*, pp 61-84.

48. Monseller, E.; Bedouelle, H. Quantitative measurement of protein stability from unfolding equilibria monitored with the fluorescence maximum wavelength. **2005**, *18*, pp 445-456.
49. Podjarny, A.; Dejaegere, A.; Kieffer, B. *Biophysical Approaches Determining Ligand Binding to Biomolecular Targets*. RSC Biomolecular Sciences. **2011**.
50. Kastritis, P.; Bonvin, A. On the binding affinity of macromolecular interactions: daring to ask why proteins interact. *J. R. Soc. Interface*. **2012**, *10*, pp 1-27.
51. Pollard, T. A Guide to Simple and Informative Binding Assays. *Molecular Biology of the Cell*. **2010**, *21*, pp 4061-4067.
52. Freeman, M.; Paik, Y.;Swift, g.; Wilczynski, R.; Wolk, S.; Yocom, K. Biodegradability of Polycarboxylates: Structure-Activity Studies. *Hydrogels and Biodegradable Polymers for Bioapplications ACS Symposium Series*. **1996**, pp 118-136.
53. Jones, S.; Thronton, J. Principles of protein-protein interactions. *Proc. Natl. Acad. Sci*. **1996**, 93, pp 13-20.
54. Roswell, S.; Pauptit, R.; Tucker, A.; Melton, R.; Blow, D.; Brick, P. Crystal structure of carboxypeptidase G_2, a bacterial enzyme with applications in cancer therapy. *Structure*. **1997**, *5*, pp 337-347.
55. Amblard, M. F., J.; Martinez, J.; Subra, G., Methods and Protocols of Modern Solid Phase Peptide Synthesis. *Molecular Biotechnology* **2006,** (33), 239-254.
56. Palomo, J., Solid-phase peptide synthesis: an overview focused on the preparation of biologically relevant peptides. *RSC Advances* **2014,** (4), 32658-32672. Kaiser, E.; Colescott, R. L.; Bossinger, C. D.; Cook, P. I., Color test for detection of free terminal amino groups in the solid-phase synthesis of peptides. *Anal Biochem* **1970,** (34), 595-598.10.1016/0003-2697(70)90146-6
57. Sarin, V. K.; Kent, S. B.; Tam, J. P.; Merrifield, R. B., Quantitative monitoring of solid-phase peptide synthesis by the ninhydrin reaction. *Anal Biochem* **1981,** (117), 147-157.10.1016/0003-2697(81)90704-1